J. Fluid Mech. (2017), *vol.* 829, *pp.* 345–363. © Cambridge University Press 2017
doi:10.1017/jfm.2017.545

Interfacial pattern selection in defiance of linear growth

Jason R. Picardo[1,2,†] and R. Narayanan[2]

[1]Department of Chemical Engineering, Indian Institute of Technology Madras, Chennai, TN 600036, India

[2]Department of Chemical Engineering, University of Florida, Gainesville, Fl 32608, USA

(Received 12 January 2017; revised 4 June 2017; accepted 2 August 2017; first published online 19 September 2017)

In this study, we revisit Rayleigh's visionary hypothesis (Rayleigh, *Proc. R. Soc. Lond.*, vol. 29, 1879*a*, pp. 71–97), that patterns resulting from interfacial instabilities are dominated by the fastest-growing linear mode, as we study nonlinear pattern selection in the context of a linear growth (dispersion) curve that has two peaks of equal height. Such a system is obtained in a physical situation consisting of two liquid layers suspended from a heated ceiling, and exposed to a passive gas. Both interfaces are then susceptible to thermocapillary and Rayleigh–Taylor instabilities, which lead to rupture/pinch off via a subcritical bifurcation. The corresponding mathematical model consists of long-wavelength evolution equations which are amenable to extensive numerical exploration. We find that, despite having equal linear growth rates, either one of the peak-modes can completely dominate the other as a result of nonlinear interactions. Importantly, the dominant peak continues to dictate the pattern even when its growth rate is made slightly smaller, thereby providing a definite counter-example to Rayleigh's conjecture. Although quite complex, the qualitative features of the peak-mode interaction are successfully captured by a low-order three-mode ordinary differential equation model based on truncated Galerkin projection. Far from being governed by simple linear theory, the final pattern is sensitive even to the phase difference between peak-mode perturbations. For sufficiently long domains, this phase effect is shown to result in the emergence of coexisting patterns, wherein each peak-mode dominates in a different region of the domain.

Key words: low-dimensional models, pattern formation, thin films

1. Introduction

One of oldest paradigms in interfacial pattern formation is that the wavelength with the largest linear growth rate dominates the emergent pattern. It was first propounded by Lord Rayleigh (1879*a*, 1879*b*) and has been found to hold in a variety of interfacial problems (Johns & Narayanan 2002), for example, the capillary instability of liquid jets (Rayleigh 1879*a*; Eggers 1997) and the Rayleigh–Taylor instability of a

† Present address: International Centre for Theoretical Sciences, Tata Institute of Fundamental Research, Shivakote, Bengaluru 560089, India. Email address for correspondence: jrpicardo@icts.res.in

heavy fluid overlying a light one (Yiantsios & Higgins 1989). The interfaces in these situations are often far above the instability threshold and consequently are linearly unstable to perturbations over a range of wavelengths (unstable linear modes). While a random noisy disturbance will excite the growth of all these modes, the length scale of the new interfacial state (drops or fingers) is typically dictated by a single linear mode – the one corresponding to the peak of the linear dispersion curve, i.e. a plot of the disturbance growth rate against its wavelength. That this should occur despite the influence of strong nonlinearities, which set in well before the final pattern emerges, is far from obvious. It suggests that pattern selection in these situations is primarily dictated by a difference of linear growth rates. Consequently, many basic features of the pattern can be determined by analysing the nonlinear evolution of the peak-mode alone.

In this work, we consider an unstable bi-layer fluid film for which the dispersion curve has two peaks of equal height. These peaks correspond to two distinct locally dominant modes that cannot be distinguished on the basis of linear growth rates. By studying their competition and the evolution of the resulting pattern, we aim to gain insight into the role of nonlinearity in wavelength selection.

The class of interfacial instabilities that we address are characterized by subcritical bifurcations, or subcritical instabilities, and continual growth of unstable modes, leading to interfacial rupture or pinch off. Such catastrophic growth is in stark contrast to problems undergoing supercritical bifurcations, or supercritical instabilities, such as the Rayleigh–Bénard and Taylor–Couette instabilities, in which the linear growth of unstable modes is saturated by nonlinearities. The new patterned state in these supercritical instabilities emerges smoothly from the un-patterned base state, as a control parameter is varied past the instability threshold. Much work has been done on the question of wavelength selection in the context of these systems (Cross & Hohenberg 1993). Busse and coworkers showed, in the context of Rayleigh–Bénard convection, that only a subset of unstable modes, surrounding the most unstable wavelength, lead to stable nonlinear steady states (Busse 1978). The selected wavelength of the nonlinear state has been shown to depend on constraints such as rigid walls and the manner in which the instability is excited (Cross & Hohenberg 1993). Raitt & Riecke (1995, 1997) considered the case of a double-peak dispersion curve in a one-dimensional system and showed that two nonlinear steady states, corresponding to the two peak-modes, can coexist as regions of distinct wavenumbers in different parts of the physical domain (domain structures). Proctor & Jones (1988) showed that if the peak wavelengths are in the ratio $1:2$, then nonlinear interaction of the peak-modes can lead to dynamic states including travelling waves, modulated waves and homoclinic orbits. Similar resonant interactions have been observed and analysed in finite two-dimensional systems, whose aspect ratios are adjusted to codimension-two points of the neutral curve (Johnson & Narayanan 1996; Echebarria, Krmpotic & Perez-Garcia 1997; Dauby, Colinet & Johnson 2000).

The results of the aforementioned studies on saturating instabilities, and the approaches used therein, are not directly applicable to the non-saturating interfacial instabilities of interest in this paper, for the following reasons. (i) The effect of saturating nonlinearity on the competition between instability modes, which emerge from the linear growth regime, is likely very different from that of the non-saturating nonlinearities present in interfacial systems. (ii) Because the instability modes saturate to nonlinear states, the question of wavelength selection in supercritical instabilities can be formulated in terms of the relative stability of the corresponding nonlinear states. If multiple nonlinear states are stable, then the relative sizes of their basins

of attraction can indicate the preferred pattern (Cross & Hohenberg 1993). Such approaches cannot be used in interfacial instabilities which do not saturate to nonlinear states. In the latter case, the dominant wavelength is decided even as the pattern continues to evolve and grow toward rupture/pinch off. In other words, whereas transients are often neglected in the study of patterns resulting from supercritical instabilities, the transient dynamics are essential to understanding pattern selection in interfacial instabilities. (iii) Due to the rupture/pinch-off event, only a finite time window is available for nonlinear effects to influence an interfacial pattern. It is conceivable, therefore, that a particular wavelength may appear in the pattern simply because nonlinear effects do not have sufficient time to suppress it in favour of another.

With these distinguishing features in mind, we attempt to understand interfacial pattern selection in the context of two-peak dispersion curves, by analysing the response of the system to various forms of disturbances. In particular, we focus on the two peak-modes and perturb them, first individually and then simultaneously. By studying the evolution of the resulting patterns, we aim to gain insight into the role of nonlinearity in the interaction between peak-modes and the extent to which it governs their mutual growth and the nature of the final pattern.

This investigation is carried out in the context of a physical system, consisting of two thin liquid layers suspended from a hot ceiling, that is unstable to long-wave Rayleigh–Taylor and Marangoni (thermocapillary) instabilities. The long-wave Marangoni instability in two-layer films was studied by Nepomnyashchy & Simanovskii (2007), who showed that the instability can be either monotonic or oscillatory, with the former case resulting in rupture of the interface. They analysed the de-wetting patterns that arise under the combined influence of Marangoni and intermolecular van der Waals forces via numerical simulations in two-dimensional periodic domains (starting from random initial perturbations). The regime of oscillatory instability was shown to result in non-rupturing oscillatory interfacial dynamics. These oscillatory states were studied in more detail in Nepomnyashchy & Simanovskii (2012), where the effect of stabilizing gravity was also included.

Our primary interest in this system is that it offers several examples of dispersion curves that have two peaks of comparable heights. The presence of two interfaces and two sources of instability enables us to tune the wavenumbers and heights of the two peaks by adjusting fluid properties. Moreover, the thinness of the films allow their dynamics to be described by just two long-wave evolution equations for the interface heights. This facilitates numerical exploration of the nonlinear dynamics of the system.

The remainder of this paper is organized as follows. The governing equations are presented in § 2, along with examples of two-peak dispersion curves. In § 3, we use the single fluid limit of our model to briefly demonstrate how the fastest-growing mode dominates patterns when the dispersion curve has a single peak. This then sets the stage for § 4, in which we present the most revealing results of our numerical calculations for the two-peak problem. These results show rather unexpected and complex inter-mode interactions that can result in either of the peak-modes dominating the pattern. A low-order ordinary differential equation (ODE) model, capable of capturing the essential qualitative features of these interactions, is presented in § 5. In the penultimate section, § 6, we extend the length of the simulation domain and investigate the emergence of coexisting patterns, in which both peak-mode patterns arise in different parts of the domain. We conclude in § 7, with a summary of the key results.

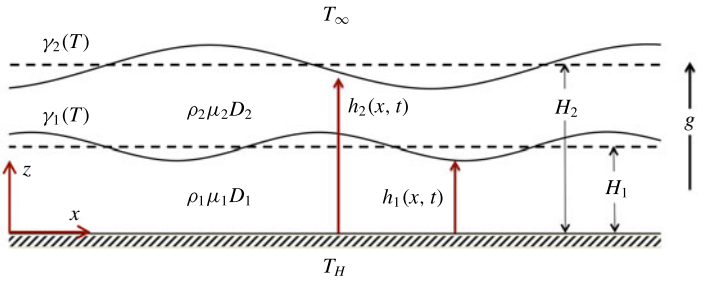

FIGURE 1. (Colour online) Schematic of the system, consisting of two liquid layers sandwiched between a hot plate at temperature T_H and a passive atmosphere at a far-field temperature T_∞. The dashed lines represent the interface positions in the unperturbed base state. $\gamma_1(T)$ is the (temperature-dependent) interfacial tension of the inter-liquid interface, while $\gamma_2(T)$ is the surface tension of the free interface of liquid 2. ρ_i, μ_i and D_i denote densities, viscosities and thermal diffusivities, respectively.

2. Two-peak interfacial dynamical system

Consider first two immiscible liquids, layered between a hot plate at temperature T_H and a passive gas at a far-field temperature of T_∞, as shown in figure 1. Liquid 1, adjacent to the plate, has a mean thickness H_1, while liquid 2 has a mean thickness $H_2 - H_1$. The interfacial tensions of both interfaces are temperature dependent: $\gamma_i = \gamma_{i\infty} - \beta_i(T - T_\infty)$ with $(i = 1, 2)$. The densities, viscosities and thermal diffusivities of the liquids are denoted by ρ_i, μ_i and D_i. Then focus on the case of thin viscous films, for which the unsteady and convective contributions to the momentum and energy balances can be neglected. Under these conditions, the two interfaces are unstable solely to long-wavelength disturbances, and λ, the length scale of longitudinal variations along x, is much larger than the local film thickness, which is of order H_2. Taking advantage of this separation of length scales, we reduce the Navier–Stokes and thermal energy balance equations to a pair of long-wave evolution equations for the interface positions (h_1 and h_2, cf. figure 1). These equations, non-dimensionalized with length scale $l_c = H_2$, velocity scale $u_c = \gamma_{2\infty}/\mu_2$ and time scale $t_c = \lambda/u_c$, are presented below:

$$\frac{\partial h_1}{\partial t} = -\frac{\partial Q_1}{\partial x}, \quad \frac{\partial h_2}{\partial t} = -\frac{\partial Q_1}{\partial x} - \frac{\partial Q_2}{\partial x} \tag{2.1a,b}$$

$$\begin{aligned} Q_1(x) \;=\; & \frac{h_1^3}{3\mu_r}\left[\gamma_r\frac{\partial^3 h_1}{\partial x^3} + Bo(\rho_r - 1)\frac{\partial h_1}{\partial x}\right] \\ & + \frac{h_1^2}{3\mu_r}\left(h_1 + \frac{3}{2}(h_2 - h_1)\right)\left[\frac{\partial^3 h_2}{\partial x^3} + Bo\frac{\partial h_2}{\partial x}\right] - \frac{Ma}{\mu_r}\frac{h_1^2}{2}\left[\beta_r\frac{\partial T_1}{\partial x} + \frac{\partial T_2}{\partial x}\right] \end{aligned} \tag{2.1c}$$

$$\begin{aligned} Q_2(x) \;=\; & \left\{\frac{(h_2 - h_1)^3}{3} + \frac{h_1(h_2 - h_1)^2}{\mu_r} + \frac{{h_1}^2(h_2 - h_1)}{2\mu_r}\right\}\left[\frac{\partial^3 h_2}{\partial x^3} + Bo\frac{\partial h_2}{\partial x}\right] \\ & + \frac{h_1^2(h_2 - h_1)}{2\mu_r}\left[\gamma_r\frac{\partial^3 h_1}{\partial x^3} + Bo(\rho_r - 1)\frac{\partial h_1}{\partial x}\right] - Ma\frac{\beta_r}{\mu_r}h_1(h_2 - h_1)\frac{\partial T_1(h_1)}{\partial x} \\ & - Ma\frac{(h_2 - h_1)}{2}\left(h_2 - h_1 + \frac{2h_1}{\mu_r}\right)\frac{\partial T_2(h_2)}{\partial x} \end{aligned} \tag{2.1d}$$

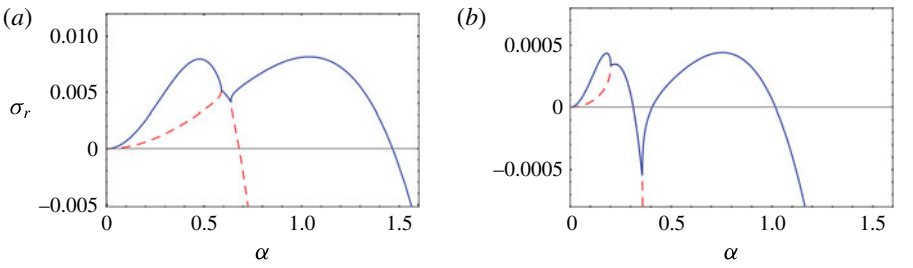

FIGURE 2. (Colour online) Two-peak linear growth curves (dispersion curves), obtained from a normal-mode linear stability analysis of (2.1), considering a quiescent base state with flat liquid layers of equal depth. The solid (blue) and dashed (red) lines correspond to the two eigenmodes, with in-phase and out-of-phase interface deflection respectively. Results are shown for two sets of parameter values, which constitute the two principal cases studied in this work. (*a*) TP1: $H_1/H_2 = 0.5$, $Bo = 0.1$, $Ma = 0.5$, $\gamma_r = 1.5$, $\beta_r = 0.85$, $\mu_r = 3$, $\rho_r = 27.697$, $Bi = 1.4$, $k_r = 1.25$; (*b*) TP2: $H_1/H_2 = 0.5$, $Bo = 0$, $Ma = 0.2$, $\gamma_r = 0.243$, $\beta_r = 2$, $\mu_r = 1.2$, $\rho_r = 2$, $Bi = 1$, $k_r = 2$.

$$T_1(h_1) = \frac{1 + Bi(h_2 - h_1)}{1 + Bi(h_2 - h_1(1 - k_r^{-1}))}, \quad T_2(h_2) = \frac{1}{1 + Bi(h_2 - h_1(1 - k_r^{-1}))}. \tag{2.1e,f}$$

Here, Q_1 and Q_2 denote the respective phase flow rate. $Ma = (T_H - T_\infty)\beta_2/\gamma_{2\infty}$ is the Marangoni number, and $Bo = H_2^2\rho_2 g/\gamma_{2\infty}$ is the Bond number. $Bi = UH_2/k_2$ is the Biot number, wherein U is the heat transfer coefficient between liquid 2 and the passive gas and k_2 is the thermal conductivity of liquid 2. μ_r, ρ_r, β_r and k_r are ratios of the respective properties of liquid 1 to liquid 2, and $\gamma_r = \gamma_{1\infty}/\gamma_{2\infty}$.

These reduced equations are derived using the weighted residual integral boundary layer method (Ruyer-Quil & Manneville 2000; Dietze & Ruyer-Quil 2013), assuming a small Reynolds number, $Re \sim O(H_2/\lambda)$, and a moderate Prandtl number, $Pr \sim O(1)$ (or the Péclet number $Pe = RePr \sim O(H_2/\lambda)$). For simplicity, we have dropped all terms of order $(H_2/\lambda)^2$ and smaller, i.e. momentum and thermal inertia, longitudinal thermal and viscous diffusion, and normal viscous surface stresses are neglected. The transverse temperature profile is a linear conduction profile that is slaved to the local interface positions. Equivalent equations can be derived using the long-wave expansion method (Oron, Davis & Bankoff 1997; Nepomnyashchy, Simanovskii & Legros 2012).

The two fluid system described by these equations is unstable to the Marangoni instability if $Ma > 0$ ($T_H > T_\infty$, $\beta > 0$). The Rayleigh–Taylor instability destabilizes the free interface if $Bo > 0$ (gravity acts in the positive z direction), while the inter-liquid interface is destabilized if $Bo > 0$ and $\rho_r > 1$, or $Bo < 0$ and $\rho_r < 1$. For the case of equal mean thicknesses of the liquids, the unstable quiescent base state corresponds to $(h_1, h_2) = (0.5, 1)$. Equations (2.1) are linearized about this state, considering infinitesimal perturbations of the form $(\hat{h}_1, \hat{h}_2)\exp(\mathrm{i}\alpha x + \sigma t)$. On solving the resulting eigenvalue problem for σ, one obtains the linear growth rate ($\sigma_r = \mathrm{Re}[\sigma]$) as a function of the wavenumber α (the corresponding plot is called the dispersion curve).

A special feature of this system is that, for appropriate combinations of fluid properties, the dispersion curve can have two peaks with comparable growth rates. Dispersion curves for two such cases, henceforth referred to as TP1 and TP2, are presented in panels 2(*a*,*b*). Here, for each wavenumber α, there are two values of σ corresponding to two distinct modes. One mode (solid blue line) corresponds

to in-phase interface deflections, wherein a crest of the top interface coincides with a crest of the bottom interface ($\hat{h}_1$ and $\hat{h}_2$ have the same sign). The other mode (red dashed line) corresponds to out-of-phase interface deflections, wherein a crest of the top interface coincides with a trough of the bottom interface ($\hat{h}_1$ and $\hat{h}_2$ have the opposite sign). In both cases, TP1 and TP2, there exists a range of wavenumbers (where the solid and dashed curves meet) for which these two modes are oscillatory and their eigenvalues form a complex-conjugate pair. However, the peaks of the dispersion curves are located in regions where the modes are non-oscillatory ($\mathrm{Im}[\sigma] = 0$). Here, the in-phase deflection mode is dominant, as its growth rate is significantly larger than that of the out-of-phase deflection mode. Therefore, in what follows we focus solely on the in-phase deflection mode (solid blue line).

Numerical solutions of (2.1) are obtained using a second-order finite difference scheme for spatial discretization. Time integration is carried out with the NDSolve routine of Mathematica®, which implements adaptive time stepping. The simulations are terminated once the thickness of either fluid reaches 0.01 times its initial value. By this stage, interface deformation ought to have progressed far enough for the nonlinear pattern to fully emerge. Moreover, the interfaces would be close to either pinching off or rupturing at the wall, and following the evolution further would require the introduction of intermolecular forces, such as van der Waals forces (Israelachvili 2011). These forces are important only for ultra-thin films and do not affect the pattern that is selected as the peak-modes of figure 2 transit from linear to nonlinear growth.

3. Nonlinear reinforcement of the fastest-growing linear mode

In this section, we use a simple example to show how the fastest-growing linear mode dominates interfacial patterns in the case of a single-peak dispersion curve. For this, we consider the Marangoni instability of a single fluid film, in the absence of gravity, obtained by setting $h_1 = 0$, $\gamma_r = 0$, $\beta_r = 0$, $\mu_r = 1$, $\rho_r = 1$, $k_r = 1$ and $Bo = 0$ in (2.1). The corresponding dispersion curve has a single peak, as depicted in panel 3(*a*). The originally flat and static interface is subjected to two separate perturbations: one corresponding to the peak-mode ($\exp(\mathrm{i}\alpha_m x)$) and another corresponding to a slower mode of twice the wavelength ($\exp(\mathrm{i}\alpha_m x/2)$). Both calculations are carried out on a periodic domain of length $4\pi/\alpha_m$. Although the initial form of the perturbed interface is quite different in the two cases (compare the two panels in figure 3*b*), the pattern that emerges at later times is indistinguishable (compare figure 3*c*,*d*).

How is it that the peak-mode is able to dominate the pattern even when it is absent from the initial perturbation? This occurs due to nonlinearities that generate the peak-mode α_m as a higher harmonic of the initial longer-wave disturbance $\alpha_m/2$. Once generated, the α_m mode quickly out paces the $\alpha_m/2$ mode and dominates the emerging pattern. In this problem, the nonlinearity originates from (i) the Marangoni surface stress that depends on interfacial temperature gradients, which in turn vary in response to the evolving interface ($Ma\partial_x[T_i(h_i)]$ in (2.1)) and (ii) viscous stresses that retard fluid flow, to an extent that increases as the film approaches the no-slip wall (terms of the form $h_i^2/2$ and $h_i^3/3$ in (2.1)). On imposing the initial perturbation of wavenumber $\alpha_m/2$, Marangoni forces begin to drain fluid symmetrically from under the single trough (cf. bottom panel of figure 3*b*). However, viscous stresses, which retard this flow, are strongest under the trough. Consequently, the largest outflow occurs not directly under the trough, but at two points located symmetrically on either side. The film height decreases faster at these locations, and the original trough

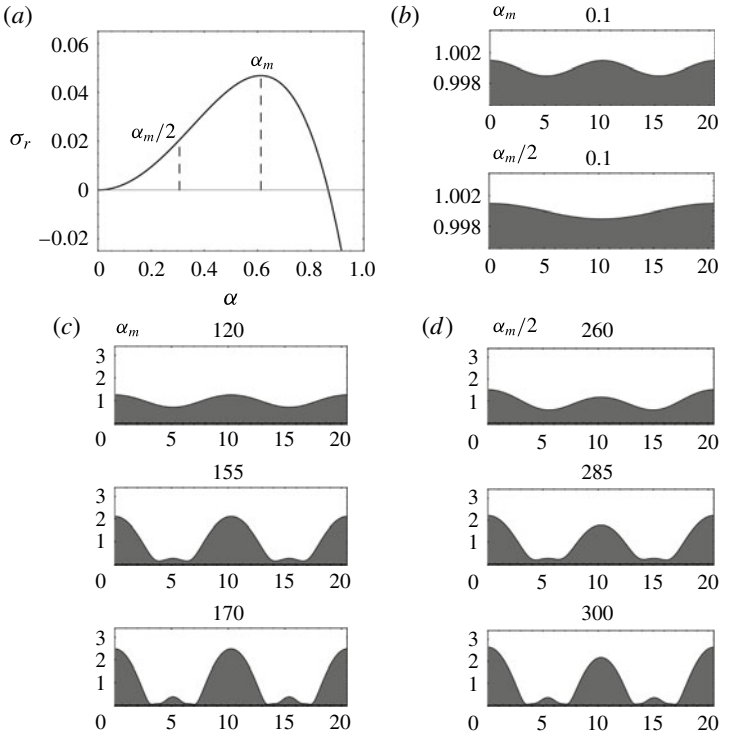

FIGURE 3. Dominance of the fastest-growing linear mode when the dispersion curve has a single peak. (*a*) Linear dispersion curve, corresponding to a single fluid on a hot plate ($Ma = 2$, $Bi = 1$, $Bo = 0$), with a peak at $\alpha_m = 0.613$. (*b*) Spatial form of linear modes corresponding to wavenumbers α_m (top panel) and $\alpha_m/2$ (bottom panel). The corresponding nonlinear evolution is shown in (*c*,*d*). The non-dimensional time is mentioned above each panel.

eventually transforms into a crest, sandwiched between two new secondary troughs (cf. top panel of figure 3*d*). This process is aided by the fact that the Marangoni flow near the original trough changes direction along with the slope of the interface, so that fluid drains out of the secondary troughs into the newly formed crest. In this manner, shorter-scale structures are generated spontaneously, a short time after imposing the initial perturbation. These include the α_m mode, which then grows much faster and quickly dominates the evolution of the interface.

The physical origin of nonlinearities capable of generating shorter-wavelength modes is different in each problem. In the capillary break-up of jets, where there are no wall effects, capillary pressure due to transverse curvature, inertia and the presence of an outer viscous fluid are all sources of structure-generating nonlinearity (Eggers 1997; Pozrikidis 1999). Whatever their origin, these nonlinearities act to reinforce the fastest linear mode so that it ultimately dominates the pattern, regardless of the amplitude of the peak-mode in the initial disturbance. This explains why it is possible to anticipate the dominant length scale in nonlinear patterns from the peak of a linear dispersion curve and why the purely linear theory of interfacial pattern formation put forth by Rayleigh (1879*a*) found reasonable agreement with experiment.

This section has shown how nonlinear effects enhance the growth of the mode with the fastest linear growth rate. In the next section, we eliminate this linear growth

bias by considering situations wherein the dispersion curve has two peaks with equal growth rates. The basic question we ask is: will both peak-modes be present in the final pattern or will nonlinearity select one of them?

4. Nonlinear selection in the context of two-peak dispersion curves

This section presents results of numerical simulations of (2.1), for cases that have dispersion curves with two peaks of comparable height. To focus attention on the peak-modes, the simulations are carried out in a finite periodic domain of length equal to the wavelength of the longer-wave peak-mode, given by $2\pi/\alpha_L$ where α_L is the wavenumber of the longer-wave peak. In the simulations, we perturb the α_L peak, as well as a commensurate mode, $\alpha_S = n\alpha_L$, which is closest to the shorter-wavelength peak. The peak-modes in figure 2 are very close to being commensurate, with $n = 2$ for case TP1 and $n = 4$ for case TP2. (This feature was a major reason for selecting these particular cases for study.) We consider small initial perturbations of the form:

$$A_0(\hat{h}_{1L}, \hat{h}_{2L})\mathrm{e}^{\mathrm{i}\alpha_L x} + B_0(\hat{h}_{1S}, \hat{h}_{2S})\mathrm{e}^{\mathrm{i}\alpha_S x+\phi} \tag{4.1}$$

where the eigenvectors $(\hat{h}_{1L}, \hat{h}_{2L})$ and $(\hat{h}_{1S}, \hat{h}_{2S})$ are of unit norm. We compare the interfacial patterns that emerge after exciting (i) only the longer-wave peak ($A_0 = 0.001, B_0 = 0$), (ii) only the shorter-wave peak ($A_0 = 0, B_0 = 0.001$) and (iii) both peaks in equal proportion ($A_0 = B_0 = 0.001$). The two peak-mode disturbances are allowed to have a phase difference ϕ. In what follows, we present results for cases TP1 and TP2 (panels (*a*,*b*) of figure 2), which serve to illustrate all the key findings of this work. The effect of extending the domain length and admitting modes longer than $2\pi/\alpha_L$ is examined later, in § 6.

Figure 4 presents results for case TP1 (cf. panel 2*a*), wherein the two peak-modes have equal linear growth rates. Column (*a*) shows the evolution of the interfacial pattern that results from perturbing the longer-wave peak-mode, $\alpha_L = 0.477$. Column (*b*) shows the result of perturbing the shorter-wave peak-mode, $\alpha_S = 2\alpha_L = 0.954$. The corresponding eigenvectors are $(\hat{h}_{1L}, \hat{h}_{2L}) = (0.253, 0.968)$ and $(\hat{h}_{1S}, \hat{h}_{2S}) = (0.820, 0.573)$. Apart from the difference in wavelengths, the qualitative nature of the two patterns is very different. The top interface is more active in the case of the α_L perturbation, and the two interfaces meet each other and pinch off, before the bottom interface meets the wall (figure 4*a*). In contrast, for the α_S disturbance, the bottom interface deforms more than the top interface, leading to rupture of the bottom interface at the wall (figure 4*b*). When both the peak-modes are perturbed simultaneously, these two contrasting patterns will grow together and possibly compete. The principle of the fastest-growing linear mode suggests that both modes should be present in the final pattern, because the two peak-modes have identical linear growth rates. However, the result shown in column (*c*) of figure 4 is in complete contradiction with this line of reasoning. The shorter-wavelength α_S mode is seen to completely dominate the interfacial pattern – all evidence of the longer-wavelength peak-mode is completely eliminated, even at relatively early times.

The situation becomes even more intriguing when the effect of a phase difference between the two peak-mode perturbations is considered. Figure 4(*d*) shows that the pattern changes completely when the perturbations are out of phase ($\phi = \pi$ in (4.1)), compared to the case when they are in phase ($\phi = 0$, cf. figure 4*c*). The nature of pinch off in figure 4(*d*) is now governed by the α_L mode, although contributions from both peak-modes are present (with α_L primarily influencing the top interface and α_S

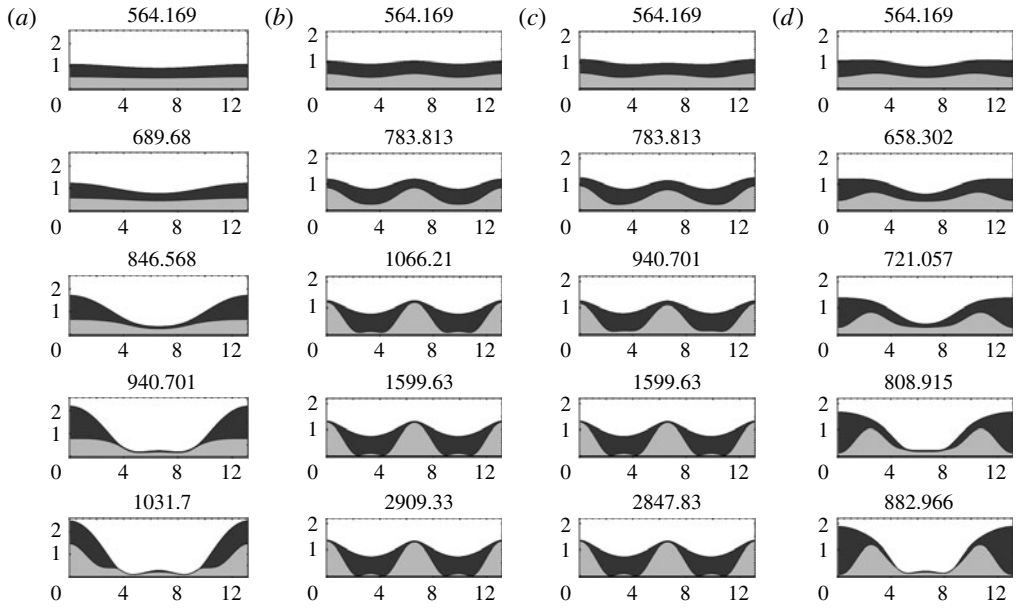

FIGURE 4. Nonlinear selection among the two peak-modes, corresponding to case TP1 (cf. figure 2*a*). Columns (*a*)–(*d*) depict the evolution of different initial perturbations: (*a*) only the longer-wavelength peak-mode ($\alpha_L = 0.477$), (*b*) only the shorter-wavelength peak-mode ($\alpha_S = 2\alpha_L = 0.954$), (*c*) equal in-phase superposition of peak-modes ($A_0 = 0.001$, $B_0 = 0.001$, $\phi = 0$ in (4.1)), (*d*) equal, out-of-phase superposition of peak-modes ($\phi = \pi$). The eigenvectors corresponding to the two peak-modes are $(\hat{h}_{1L}, \hat{h}_{2L}) = (0.253, 0.968)$ and $(\hat{h}_{1S}, \hat{h}_{2S}) = (0.820, 0.573)$. The non-dimensional time corresponding to each interfacial pattern is mentioned above the respective panel.

impacting the bottom interface). Linear stability calculations are unaffected by phase differences, and consequently, the linear dispersion curve is powerless to explain such phase-dependent pattern evolution.

In hindsight, the influence of a phase difference can be understood by comparing the early evolution of the two independent perturbations to the peak-modes. The α_L mode causes the interfaces to move downward at the centre of the domain (figure 4*a*), whereas the α_S mode causes the interfaces to move upward at the same location (figure 4*b*). Therefore, the two modes compete when they are excited in phase, with the result that α_S dominates (figure 4*c*). On the other hand, out-of-phase disturbances can grow together and coexist in the final pattern, as seen in figure 4(*d*). Thus, the influence of phase differences is tied to the interaction between crests and troughs of the two peak-mode patterns. By this logic, phase differences should cease to matter when the two peak-modes have very different wavelengths. In this case, a trough of the longer-wave pattern will overlap with several crests and troughs of the shorter-wave pattern, and the net interaction of the two patterns should not be significantly influenced by the phase difference. This holds true for case TP2 (wherein $\alpha_S = 4\alpha_L$, cf. panel 2*b*), as demonstrated by panels 5(*a–d*). Panels 5(*a*,*b*) show the final pattern resulting from independent perturbations of the α_L and α_S modes respectively. Panels 5(*c*,*d*) show the results of in-phase and out-of-phase superposed peak-mode perturbations. As expected, the phase difference does not significantly affect the

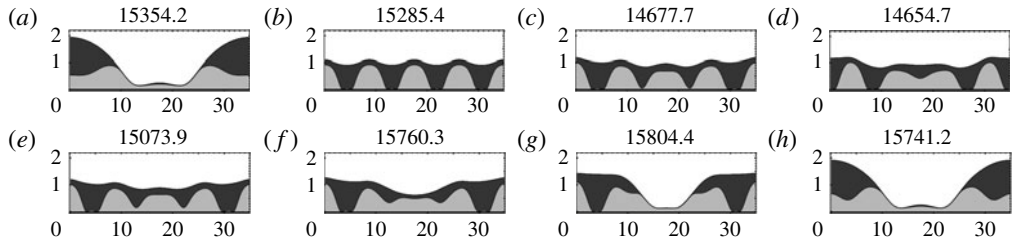

FIGURE 5. The influence of phase difference and a counter-example to Rayleigh's principle in the context of case TP2 (cf. figure 2*b*). Each panel shows the final pattern obtained just before terminating the simulation, along with the corresponding non-dimensional time (mentioned above each panel). In (*a–d*), the two excited peak-modes, $\alpha_L = 0.196$ and $\alpha_S = 4\alpha_L = 0.784$, have equal linear growth rates of 0.00043. The eigenvectors corresponding to the two peak-modes are $(\hat{h}_{1L}, \hat{h}_{2L}) = (0.165, 0.986)$ and $(\hat{h}_{1S}, \hat{h}_{2S}) = (0.993, 0.120)$. The perturbations in each panel are: (*a*) only α_L, (*b*) only α_S, (*c*) in-phase superposition ($A_0 = 0.001$, $B_0 = 0.001$, $\phi = 0$ in (4.1)), (*d*) out-of-phase superposition ($\phi = \pi$). Panels (*e–h*) show how the final pattern for equal in-phase perturbations ($A_0 = 0.001, B_0 = 0.001, \phi = 0$) changes as the growth rate of the shorter-wave peak-mode (α_S) is reduced in four stages (by increasing the interfacial tension ratio γ_r): (*e*) 0.00042, (*f*) 0.00040, (*g*) 0.00038, (*h*) 0.00033.

qualitative nature of the pattern, which is completely dominated by the shorter-wave α_S peak-mode.

The erstwhile dominant peak-mode (shorter-wavelength peak) continues to dominate even when its growth rate is slightly reduced. This result is demonstrated by panel 5(*e*), which corresponds to a slightly modified case of TP2 (cf. panel 2*b*), in which the α_S mode has a slightly smaller growth rate than the α_L mode (cf. the caption of figure 5). This is a definite counter-example to Rayleigh's paradigm of the fastest-growing linear mode, because in this case the mode with a smaller linear growth rate dominates the pattern! Of course, as the growth rate of the α_S mode is decreased further (panels 5*f–h*), the system eventually behaves like one with a single-peak dispersion curve and the α_L mode sets the pattern (compare panels 5*a*,*h*). A similar result is found for in-phase perturbations of the peak-modes of case TP1. The shorter α_S mode (cf. figure 4*b*) continues to dominate even when its growth rate is slightly reduced. Further reduction, however, eventually leads to the longer α_L peak-mode (cf. figure 4*a*) dominating.

5. Low-order ODE model: a truncated Galerkin approach

The previous section has demonstrated that interfacial pattern evolution cannot be anticipated from linear stability theory alone, in cases where the dispersion curve has two peaks of comparable height. Numerical investigations tell us that either peak-mode can dominate the pattern and that the outcome may also depend on the phase difference between initial perturbations, but not always. Anticipating the final pattern requires one to account for nonlinear interactions between the peak-modes. At the same time, full numerical simulations are computationally expensive and may be unfeasible in many situations, especially when different types of perturbations must be considered. An alternative is to develop a low-order ordinary differential equation model that accounts for only the key interactions between peak-modes, in order to

predict which of the two dominates. In systems close to the onset of instability, at codimension-two supercritical points, such amplitude equations have been derived using asymptotic techniques like multiple scale expansions (Cross & Hohenberg 1993) or the centre manifold reduction (Carini, Auteri & Giannetti 2015; Roberts 2015). In this work, we are primarily concerned with systems that are far above the instability threshold and undergoing subcritical bifurcations. Moreover, we wish to describe the evolution of the most unstable peak-modes and not those close to the cutoff neutral wavenumber. Therefore, rather than applying a strict asymptotic procedure, we derive a low-order model by carrying out a Galerkin projection of the governing equations (2.1) onto a set of judiciously selected modes (Balmforth, Provenzale & Whitehead 2001).

By comparing various truncated models with full simulations of the partial differential equation (PDE) model (2.1), we have found that the lowest-order ODE model capable of adequately describing the system is one based on three modes – the two peak-modes and a third mode that facilitates their interaction. The interface heights are represented as a combination of these modes, as follows:

$$\begin{bmatrix} h_1 \\ h_2 \end{bmatrix} = A(t) \begin{bmatrix} \hat{h}_{1,L} \\ \hat{h}_{2,L} \end{bmatrix} \mathrm{e}^{\mathrm{i}(\alpha_L)x} \mathrm{e}^{\mathrm{i}\phi_1(t)} + B(t) \begin{bmatrix} \hat{h}_{1,S} \\ \hat{h}_{2,S} \end{bmatrix} \mathrm{e}^{\mathrm{i}(\alpha_S)x} \mathrm{e}^{\mathrm{i}\phi_2(t)} + C(t) \begin{bmatrix} \hat{h}_{1,L} \\ \hat{h}_{2,L} \end{bmatrix} \mathrm{e}^{\mathrm{i}(\alpha_S)x} \mathrm{e}^{\mathrm{i}\phi_3(t)} + \mathrm{c.c.} \tag{5.1}$$

Here $\alpha_S = n\alpha_L$, where n is an integer, as we are considering commensurate peak-modes. The first two modes, with amplitudes $A(t)$ and $B(t)$, correspond to the longer-wave and shorter-wave peak-modes respectively. The third mode, with amplitude $C(t)$, has the eigenvector of the longer-wave peak-mode ($\hat{h}_{1L}$, $\hat{h}_{2L}$) but the spatial variation of the shorter-wave peak-mode ($\mathrm{e}^{(\mathrm{i}\alpha_S)x}$). This mode is especially important when the two eigenvectors ($\hat{h}_{1L}$, $\hat{h}_{2L}$) and ($\hat{h}_{1S}$, $\hat{h}_{2S}$) are orthogonal. In this case, a nonlinear term (quadratic if $n = 2$, as in case TP1) acting on the α_L mode will not make any contribution to the equation for the α_S mode, after Galerkin projection. The third mode, on the other hand, will always be affected nonlinearly by the α_L mode while simultaneously contributing to the equation for the α_S mode, thereby facilitating communication between the two peak-modes. The importance of considering this third interaction mode is illustrated in figure 8, to be introduced later.

Expression (5.1) is substituted into (2.1), which is then projected onto the three modes. Projection involves taking the scalar product of the equations with the mode, followed by spatial integration. After equating real and imaginary parts, this results in six nonlinear coupled ODEs for the amplitudes $A(t)$, $B(t)$ and $C(t)$ and the phases $\phi_1(t)$, $\phi_2(t)$ and $\phi_3(t)$. For simplicity, only the lowest-order nonlinear terms that enable the peak-modes to interact are retained. For case TP1, second-order terms are required, because the peak-mode wavenumbers are in a 1 : 2 ratio, whereas, terms up to fourth order must be retained for case TP2 where the peak-modes are in a 1 : 4 ratio (cf. panels 2*a*,*b*). (It was verified that higher-order terms do not modify the prediction of the dominant mode.) The following initial conditions were used, to simulate the evolution of an initial perturbation to both peak-modes: $A = B = 0.001$, $C = 0$, $\phi_1 = 0$, $\phi_2 = \phi$ and $\phi_3 = 0$. Here, ϕ is the phase difference between the initial peak-mode perturbations, as defined in (4.1), and the disturbance amplitude of 0.001 is the same as that used in the simulations of the PDE model (2.1).

Figure 6 compares the prediction of this three-mode ODE model (dashed lines) with the amplitudes extracted from simulations of the PDE model (solid lines), for

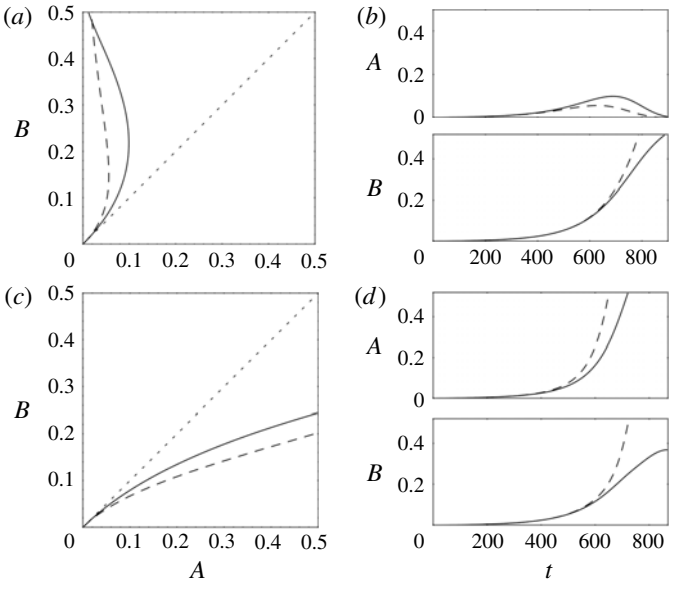

FIGURE 6. Low-dimensional description of the evolution of the peak-modes for case TP1 of panel 2(*a*). $A(t)$ is the amplitude of the longer-wave peak-mode while $B(t)$ is the amplitude of the shorter-wave peak-mode. The solid lines represent the amplitudes of the peak-modes (cf. (5.1)) extracted from the simulation of the PDE model (2.1), while the dashed lines are the predictions of the three-mode ODE model. Panels (*a*,*b*) depict the phase plane trajectory and temporal evolution of the amplitudes, for the case of in-phase peak-mode perturbations ($\phi = 0$ in (4.1)). Panels (*c*,*d*) correspond to out-of-phase peak-mode perturbations ($\phi = \pi$ in (4.1)). The associated spatial evolution is presented in panels 4(*c*,*d*), respectively. In (*a*,*c*), time progresses along the phase plane trajectories, starting at the origin. The dotted lines in these panels are diagonals.

case TP1 (cf. panel 2*a*). Panels 6(*a*,*c*) depict phase plane plots for in-phase ($\phi = 0$) and out-of-phase ($\phi = \pi$) initial peak-mode perturbations, while panels 6(*b*,*d*) show the corresponding temporal evolution. The ODE model is able to capture the qualitative features of the evolution of the peak-modes, including the influence of the phase difference. It successfully predicts the dominance of the shorter-wave peak-mode for in-phase perturbations (panel 6*a*), and the co-existence of both peak-modes for out-of-phase perturbations (with the longer-wave peak-mode playing a larger role, cf. panel 6*c*). Quantitative accuracy of the model is, however, restricted to small values of the amplitudes (panels 6*b*,*d*). As the amplitudes of the peak-modes increase, the neglected high-order interaction terms (cubic and greater in this case) become increasingly relevant. Moreover, higher harmonics of the peak-modes get excited and may begin to influence the growth of the peak-modes. These effects cannot be captured by the truncated three-mode ODE model. The fact that the ODE model is able to predict the dominant mode, in spite of these limitations, implies that pattern selection is largely determined by direct nonlinear interaction between the peak-modes, at a relatively early stage of their evolution.

Figure 7 presents results for case TP2 (cf. panel 2*b*). The ODE model successfully predicts the dominant mode to be the shorter-wave peak-mode, for both in-phase (panels 7*a*,*b*) and out-of-phase perturbations (panels 7*c*,*d*). If the interfacial tension

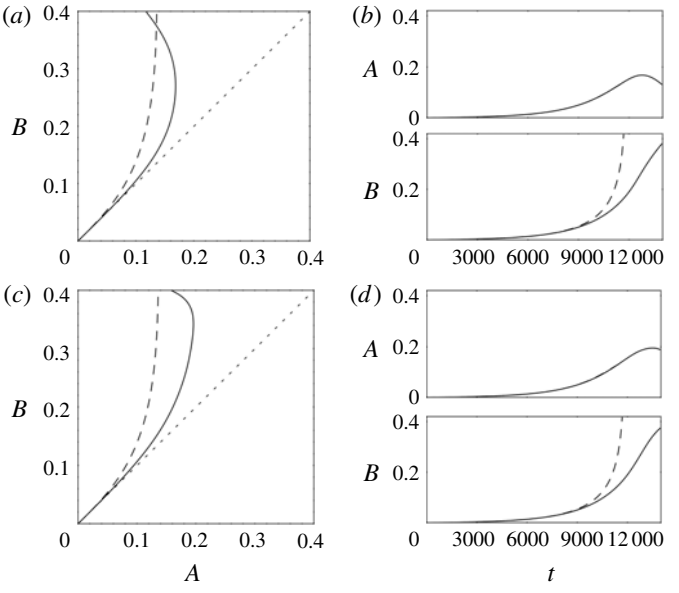

FIGURE 7. Low-dimensional description of the evolution of the peak-modes for case TP2 of panel 2(*b*). $A(t)$ is the amplitude of the longer-wave peak-mode while $B(t)$ is the amplitude of the shorter-wave peak-mode. The solid lines represent the amplitudes of the peak-modes (cf. (5.1)) extracted from the simulation of the PDE model (2.1), while the dashed lines are the predictions of the three-mode ODE model. Panels (*a*,*b*) depict the phase plane trajectory and temporal evolution of the amplitudes, for the case of in-phase peak-mode perturbations ($\phi = 0$ in (4.1)). Panels (*c*,*d*) correspond to out-of-phase peak-mode perturbations ($\phi = \pi$ in (4.1)). The final spatial patterns corresponding to these two cases are presented in panels 5(*c*,*d*), respectively. The dotted lines in (*a*,*c*) are diagonals.

ratio is increased so as to slightly decrease the linear growth rate of the shorter-wave peak-mode, the ODE model continues to predict the dominance of the shorter-wave mode, in agreement with panels 5(*c*,*e*).

Similar to the results for case TP1 (cf. figure 6), the ODE model is quantitatively accurate only for small amplitudes. Beyond $t \approx 11\,000$, the ODE prediction for $B(t)$ increases much more rapidly than the PDE results (cf. panels 7*b*,*d*). In fact the ODE solution displays a singularity at $t \approx 11\,800$. This non-physical behaviour may be cured by including additional modes in the ODE model. However, this is not necessary if the primary goal is to predict which peak-mode is dominant in the final pattern.

A particularly encouraging aspect of the ODE model is its ability to capture the influence of the phase difference between perturbations, which significantly impacts the final pattern in case TP1 (compare panel 4*c* with 4*d* and panel 6*a* with 6*c*). As the model contains only three modes, it may be possible to gain insight into inter-peak interaction and the role of phase differences, by a direct examination of the ODEs. To obtain the equations for case TP1, the parameter values corresponding to case TP1 (cf. caption of panel 2*a*) are substituted into the full PDE model (2.1), which is then projected onto the three modes (5.1). The calculations are carried out with the aid of symbolic computing in Mathematica®. The equations take on a relatively simple form if we restrict ourselves to in-phase and out-of-phase perturbations ($\phi = 0, \pi$ in (4.1)):

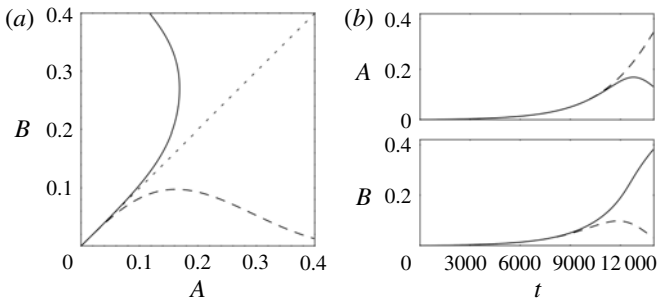

FIGURE 8. Demonstration of the importance of the interaction mode (of amplitude $C(t)$ in (5.1)) in the reduced-order ODE model. Phase plane orbits (a) and the temporal evolution (b) of the peak-modes are presented, for the system in panel 2(b), considering in-phase perturbations. (a) The solid lines are obtained from a simulation of the PDE model (2.1) and are identical to the solid lines in panels 7(a,b). The dashed lines are predictions of a two-mode ODE model that does not include the interaction mode. These predictions should be compared with the dashed lines in 7(a,b), obtained from the three-mode ODE model which retains the interaction mode. While the three-mode ODE model is qualitatively accurate and predicts the dominance of the shorter-wave peak-mode, the two-mode ODE model fails entirely and predicts the opposite result.

$$\frac{\mathrm{d}A}{\mathrm{d}t} = \sigma A - m_1 AC - m_2 AB\cos(\phi) \tag{5.2a}$$

$$\frac{\mathrm{d}B}{\mathrm{d}t} = \sigma B - m_3 C\sec(\phi) - m_4 A^2\sec(\phi) \tag{5.2b}$$

$$\frac{\mathrm{d}C}{\mathrm{d}t} = \omega C + m_5 A^2 \tag{5.2c}$$

Here, σ and ω are the individual linear growth rates of each mode and m_i are positive constants. The values of these coefficients are specific to the parameter values of case TP1: $\sigma = 0.008$, $\omega = -0.063$, $m_1 = 0.137$, $m_2 = 0.053$, $m_3 = 0.0003$, $m_4 = 0.002$, $m_5 = 0.012$. The coefficient σ is the same for the two peak-mode amplitudes A and B because we have used parameter values corresponding to case TP1, for which the peak-modes have equal linear growth rates.

The other terms in (5.2) account for inter-mode interaction, and include nonlinearities up to second order (the lowest order required for nonlinear interaction between the peak-modes, which are in a 1 : 2 wavelength ratio). Particularly important are the third terms on the right-hand side of (5.2a) and (5.2b). For in-phase perturbations ($\phi = 0$), these terms show that the two peak-modes compete, with the growth of B suppressing that of A (via $-m_2AB$) and *vice versa* (via $-m_4A^2$). Because $m_2 > m_4$, in this case, the shorter-wave mode dominates the pattern. For out-of-phase perturbations ($\phi = \pi$), on the other hand, the sign of these terms reverse, indicating that the two modes cooperate and allow each other to coexist in the final pattern. This competition/cooperation stems from the manner in which crests and troughs of the two peak-modes overlap, as was discussed pictorially in § 4.

We have tested the three-mode ODE model for other cases as well, and have found similar positive results, with regard to the qualitative nature of the peak-mode interaction and the prediction of the dominant mode. For the sake of brevity, we only present one additional example in appendix A, for which the peak-mode wavelengths are in a 1 : 3 ratio. In this particular case, both modes play nearly equal roles in establishing the final pattern and neither is able to dominate.

We conclude this section by demonstrating the importance of including the interaction mode, of amplitude $C(t)$, in the ODE model. This mode is particularly important for case TP2 (cf. panel 2*b*), because the eigenvectors corresponding to the peak-modes are close to being orthogonal $(\hat{h}_{1L}, \hat{h}_{2L}) = (0.165, 0.986)$ and $(\hat{h}_{1S}, \hat{h}_{2S}) = (0.993, 0.120)$. In this case, although fourth-order nonlinearities would generate a harmonic of the longer-wave mode (of wavenumber α_L) with a spatial variation matching the shorter-wave mode (of wavenumber $4\alpha_L$), its projection onto the latter would be very small. Thus a two-mode ODE model, with just the peak-modes, will not be able to capture their interaction. This is shown by the results in figure 8, which corresponds to in-phase perturbations of the peak-modes of case TP2. The two-mode model completely fails, as it predicts the dominance of the longer-wave peak-mode, when in fact the shorter-wave mode dominates.

This deficiency of the two-mode model has been overcome by including just one extra mode – the interaction mode, which combines the spatial variation of the shorter-wave peak-mode (α_S) with the eigenvector of the longer-wave peak-mode ($\hat{h}_{1L}, \hat{h}_{2L}$) (cf. (5.1)). The longer-wave mode can strongly excite the interaction mode, which in turn influences the evolution of the shorter-wave peak-mode via linear coupling. For case TP1, this interaction is represented by the second terms on the right-hand side of (5.2*c*) and (5.2*b*). These terms do not play a major role in case TP1 because the eigenvectors are far from being orthogonal, $(\hat{h}_{1L}, \hat{h}_{2L}) = (0.253, 0.968)$ and $(\hat{h}_{1S}, \hat{h}_{2S}) = (0.820, 0.573)$, which enables a strong direct interaction between the peak-modes. In contrast, the interaction mode is important in case TP2 where direct interaction is weak, and it is only by including the interaction mode that the ODE model is able to successfully identify the dominant peak-mode (compare panel 7*a* with 8*a*).

6. Coexisting patterns on long domains

In the numerical simulations of § 4, the non-dimensional domain length (L) was chosen to be just large enough to accommodate the longer-wave peak-mode, i.e. $L = 2\pi/\alpha_L$. Increasing the domain length further admits modes of larger wavelengths. Due to their smaller growth rates, one may expect them to be dominated by the peak-modes. However, these long-wavelength modes may be able to affect the interfacial pattern by modulating the local phase difference between the peak-modes. In situations where the pattern depends on the phase difference, such as case TP1 (cf. panels 4*c*,*d*), this phase modulation could result in the emergence of coexisting patterns on long domains.

To demonstrate this, we consider an extended domain of $L = 4 \times 2\pi/\alpha_L$ for case TP1 (cf. panel 2*a*). This domain is four times that of figure 4. Both peak-modes are perturbed with equal amplitudes ($A_0 = B_0 = 0.001$ in (4.1)), but with a spatially varying phase difference $\phi(x)$ such that the peak-modes are in phase on the left half of the domain and out of phase on the right half. The function $\phi(x)$ is plotted in panel 9(*a*) and its exact form is given below:

$$\phi(x) = \frac{\pi}{2}\left(1 + \frac{2}{\pi}\arctan(4(x - L/2))\right). \tag{6.1}$$

The interfacial pattern that results from this perturbation is shown in panel 9(*b*). The left half of the domain resembles the pattern in panel 4(*c*), wherein the bottom interface approaches rupture at the wall. The right half of the domain resembles panel 4(*d*), wherein the two interfaces approach pinch off. The patterns transition

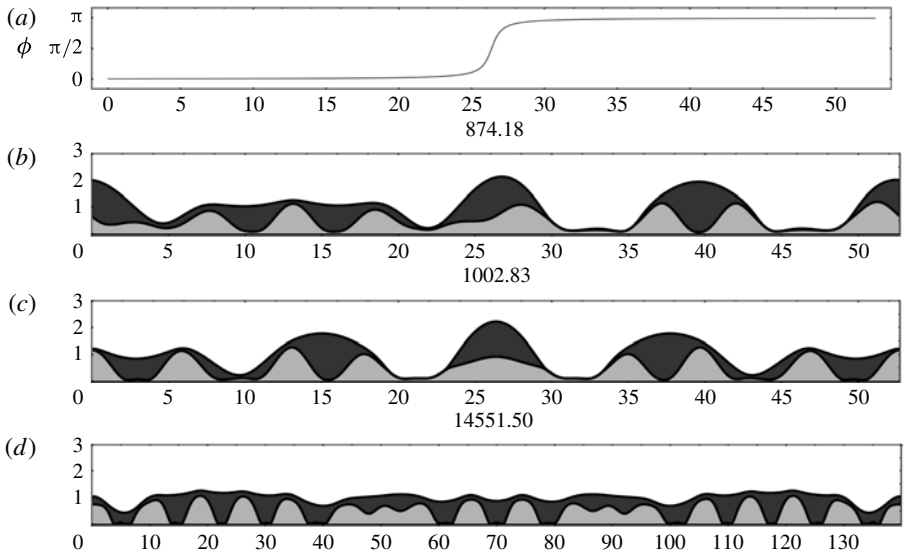

FIGURE 9. Emergence of coexisting patterns on a long domain, $L = 4 \times 2\pi/\alpha_L$. (*a*) The spatially varying phase difference $\phi(x)$ used in the initial perturbation (4.1) to the peak-modes. (*b*) The coexisting pattern that results from perturbing the peak-modes of case TP1 (panel 2*a*) with the spatially varying phase difference given in (*a*). (*c*) The result of perturbing all admissible unstable modes of case TP1 (with wavenumbers $\alpha = 2m\pi/L$, $m = 1, 2, 3...$), without any phase differences. Here the relative phase between the peak-modes is modulated naturally, due to the excitation of the longest wavelengths in the domain. (*d*) Result of a similar perturbation as that in (*c*), but for case TP2 (cf. panel 2*b*) wherein the phase difference between peak-mode perturbations does not affect the pattern appreciably.

from one to the other at the centre of the domain. The shorter-wave peak dominates on the left half (cf. panel 4*a*) while the signature of the longer-wave peak is apparent on the right half (cf. panel 4*b*), in accordance with the influence of the phase difference on inter-peak competition (cf. § 5).

That such modulation of the local phase difference between peak-modes can arise naturally, due to the influence of very-long-wavelength modes, is demonstrated by panel 9(*c*). Here all admissible wavelengths ($\alpha = 2m\pi/L = m\alpha_L/4$, with $m = 1, 2, 3\ldots$), with positive linear growth rates, are excited equally and in phase. The signature of the longer-wave peak-mode can be seen in the centre of the domain while the shorter-wave peak-mode dominates near the two ends of the periodic domain.

Panel 9(*d*) shows the results of a similar calculation for case TP2 (cf. panel 2*b*) where the phase difference between peak-mode perturbations does not appreciably affect the pattern (cf. panel 5*c*,*d*). Here, although the interface is less deformed in certain regions of the domain, the shorter-wave peak-mode (panel 5*b*) dominates throughout and there is no signature of the longer-wave peak-mode (panel 5*a*). These results show that coexisting patterns are likely to arise for cases wherein the phase difference between peak-modes significantly influences their interaction.

It should be noted that systems undergoing supercritical bifurcations also exhibit coexisting patterns, which are called domain structures (Raitt & Riecke 1995, 1997). This was demonstrated by Raitt & Riecke (1995) for a fourth-order (in space) Ginzburg–Landau equation that has a two-peak linear dispersion curve. Here the

peak-modes saturate to nonlinear states with distinct wavelengths, which exist alongside one another in different regions of the domain. In the absence of a rupture-like catastrophe, these systems can evolve indefinitely. Therefore, for a coexisting pattern to be observed it is necessary for the state with coexisting patterns to be stable to perturbations. Otherwise, one pattern would invade the other and lead to a uniformly patterned state. This issue does not arise in the interfacial system under study, because rupture/pinch off occurs before the patterns arising in different regions can influence each other significantly.

7. Conclusions

This work has focused on pattern selection in interfacial problems that are characterized by subcritical bifurcations and nonlinear growth that leads to rupture/pinch off. In systems with single-peak linear dispersion curves, the characteristic scales of the final pattern are often set by the mode with the fastest linear growth rate. This occurs even though the system if far above the instability threshold because nonlinearity reinforces the growth of the peak-mode. The situation is very different, however, when the dispersion curve has two peaks of comparable heights. This work has shown that either of the two peak-modes can completely dominate the pattern, even if they have identical linear growth rates. Furthermore, the pattern remains unaltered on reducing the growth rate of the dominant peak-mode, within a finite margin. This is in direct contradiction of the usual assertion that the fastest-growing linear mode dominates the pattern. Such unexpected behaviour results from nonlinear interaction between the peak-modes, which may be influenced by the phase difference between the initial peak-mode perturbations.

To capture the essentials of the peak-mode interaction, we have developed a simple three-mode ODE model, which has proven to be remarkably effective in predicting the qualitative nature of the emergent pattern. This model is obtained by projecting the governing nonlinear partial differential equations onto the two peak-modes and an additional interaction mode, which is particularly important when the peak-mode eigenvectors are orthogonal. This methodology can be applied to any two-peak system, and will be especially useful in computationally demanding problems, for which running a host of direct numerical simulations is unfeasible.

The possible dependence of the final pattern on the phase difference between peak-modes has been shown to result in the emergence of coexisting patterns, when the domain is sufficiently large. The additional long-wavelength modes admitted by increasing the domain size have the effect of modulating the local phase difference between the peak-modes, which in turn allows distinct patterns to emerge in different parts of the domain.

Acknowledgements

The authors thank D. S. Pillai for stimulating discussions. J.R.P. is thankful for the opportunity to carry out research at the University of Florida provided by the Fulbright-Nehru fellowship. Funding from NSF-0968313 and the Institute of Advanced Study at Durham University is also gratefully acknowledged.

Appendix

An additional case of a two-peak dispersion curve in briefly considered in this appendix. This case differs from those in figure 2 in that the two peaks of the

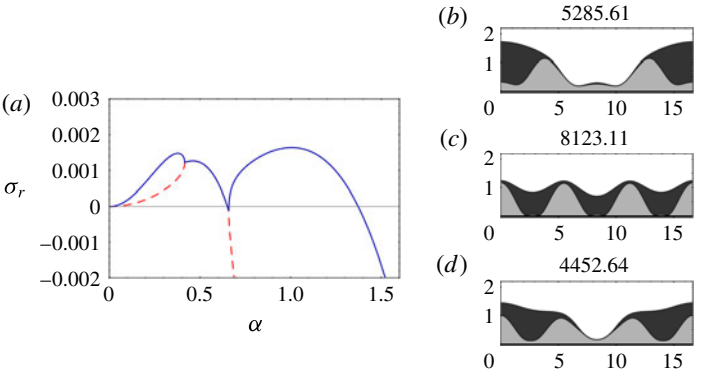

FIGURE 10. (Colour online) Case with peak-modes in a 1 : 3 wavelength ratio. (*a*) Linear growth curve: the solid (blue) and dashed (red) lines correspond to the two eigenmodes, with in-phase and out-of-phase interface deflection respectively. Panels (*b–d*) present the final spatial pattern resulting from various initial perturbations: (*b*) only the longer-wave peak-mode ($\alpha_L = 0.377$), (*c*) only the shorter-wave peak-mode ($\alpha_S = 3\alpha_L = 1.131$), (*d*) equal in-phase perturbation of both peak-modes ($A_0 = 0.001$, $B_0 = 0.001$, $\phi = 0$ in (4.1)). The eigenvectors corresponding to the two peak-modes are $(\hat{h}_{1L}, \hat{h}_{2L}) = (0.017, 1.000)$ and $(\hat{h}_{1S}, \hat{h}_{2S}) = (0.937, 0.348)$. The non-dimensional time corresponding to each pattern in (*b*) to (*c*) is mentioned above the respective panel. Parameter values: $H_1/H_2 = 0.5$, $Bo = 0.2$, $Ma = 0.5$, $\gamma_r = 1.5$, $\beta_r = 0.9$, $\mu_r = 24$, $\rho_r = 13.0386$, $Bi = 1.4$, $k_r = 0.4$.

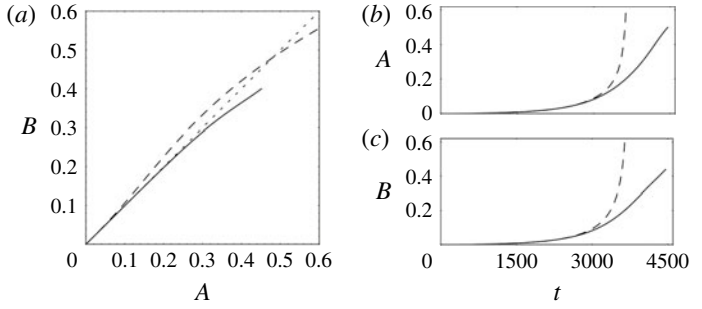

FIGURE 11. Low-dimensional description of the evolution of the peak-modes for the case in panel 10(*a*), considering in-phase perturbations. $A(t)$ is the amplitude of the longer-wave peak-mode while $B(t)$ is the amplitude of the shorter-wave peak-mode. The solid lines represent the amplitudes of the peak-modes (cf. (5.1)) extracted from the simulation of the PDE model (2.1), while the dashed lines are the predictions of the three-mode ODE model. Panels (*a*,*b*) depict the phase plane trajectory and temporal evolution of the amplitudes. The final spatial patterns corresponding to these two cases are presented in panels 10(*c*,*d*), respectively. The dotted line in (*a*) is a diagonal.

dispersion curve are close to a ratio of 1 : 3, as shown in panel 10(*a*). For the numerical simulations, we perturb the longer-wave peak-mode ($\alpha_L = 0.377$) and a commensurate shorter-wave mode ($\alpha_S = 3\alpha_L = 1.131$) that is close to the second peak. Both peak-modes have the same linear growth rate. The final spatial patterns that result from perturbations corresponding to (*a*) only the longer-wave peak-mode, (*b*) only the shorter-wave peak-mode, and (*c*) equal in-phase superposition of both

peak-modes are presented in panels 10(*b–d*). The final pattern contains significant signatures of both peak-modes, and neither is able to dominate over the other.

The low-order ODE model captures this behaviour well, as shown in figure 11, which compares the prediction of the three-mode ODE model with the PDE simulation. However, as in cases TP1 (cf. figure 6) and TP2 (cf. figure 7), quantitative accuracy is limited to small values of the peak-mode amplitudes. The phase difference between peak-mode perturbations does not influence the final pattern appreciably, in this case.

REFERENCES

BALMFORTH, N. J., PROVENZALE, A. & WHITEHEAD, J. A. 2001 The language of pattern and form. In *Geomorphological Fluid Mechanics* (ed. N. J. Balmforth & A. Provenzale), Springer.

BUSSE, F. H. 1978 Non-linear properties of thermal convection. *Rep. Prog. Phys.* **41**, 1929–1967.

CARINI, M., AUTERI, F. & GIANNETTI, F. 2015 Centre-manifold reduction of bifurcating flows. *J. Fluid Mech.* **767**, 109–145.

CROSS, M. C. & HOHENBERG, P. C. 1993 Pattern formation outside of equilibrium. *Rev. Mod. Phys.* **65** (3), 851–1112.

DAUBY, P. C., COLINET, P. & JOHNSON, D. 2000 Theoretical analysis of a dynamic thermoconvective pattern in a circular container. *Phys. Rev.* E **61**, 2663–2668.

DIETZE, G. F. & RUYER-QUIL, C. 2013 Wavy liquid films in interaction with a confined laminar gas flow. *J. Fluid Mech.* **722**, 348–393.

ECHEBARRIA, B., KRMPOTIC, D. & PEREZ-GARCIA, C. 1997 Resonant interactions in Bénard–Marangoni convection in cylindrical containers. *Physica* D **99**, 487–502.

EGGERS, J. 1997 Nonlinear dynamics and breakup of free-surface flows. *Rev. Mod. Phys.* **69**, 865–930.

ISRAELACHVILI, J. N. 2011 *Intermolecular and Surface Forces*, 3rd edn. Academic.

JOHNS, L. E. & NARAYANAN, R. 2002 *Interfacial Instability*. Springer.

JOHNSON, D. & NARAYANAN, R. 1996 Experimental observation of dynamic mode switching in interfacial-tension-driven convection near a codimension-two point. *Phys. Rev.* E **54** (4), R3102–R3104.

NEPOMNYASHCHY, A. A. & SIMANOVSKII, I. B. 2007 Marangoni instability in ultrathin two-layer films. *Phys. Fluids* **19** (12), 122103.

NEPOMNYASHCHY, A. A. & SIMANOVSKII, I. B. 2012 Nonlinear marangoni waves in a two-layer film in the presence of gravity. *Phys. Fluids* **24** (3), 032101.

NEPOMNYASHCHY, A., SIMANOVSKII, I. & LEGROS, J. C. 2012 *Interfacial Convection in Multilayer Systems*, 2nd edn. Springer.

ORON, A, DAVIS, S. H. & BANKOFF, S. G. 1997 Long-scale evolution of thin liquid films. *Rev. Mod. Phys.* **69** (3), 931–980.

POZRIKIDIS, C. 1999 Capillary instability and breakup of a viscous thread. *J. Engng Maths* **36**, 255–275.

PROCTOR, M. R. E. & JONES, C. A. 1988 The interaction of two spatially resonant patterns in thermal convection. Part 1. Exact 1:2 resonance. *J. Fluid Mech.* **188**, 301–335.

RAITT, D. & RIECKE, H. 1995 Domain structures in fourth-order phase and Ginzburg–Landau equations. *Physica* D **82** (1), 79–94.

RAITT, D. & RIECKE, H. 1997 Parametric forcing of waves with a nonmonotonic dispersion relation: domain structures in ferrofluids. *Phys. Rev.* E **55**, 5448–5454.

RAYLEIGH, LORD 1879*a* On the capillary phenomena of jets. *Proc R. Soc. Lond.* **29**, 71–97.

RAYLEIGH, LORD 1879*b* On the instability of liquid jets. *Proc. Lond. Math. Soc.* **10**, 4–13.

ROBERTS, A. J. 2015 *Model Emergent Dynamics in Complex Systems*. SIAM.

RUYER-QUIL, C. & MANNEVILLE, P. 2000 Improved modeling of flows down inclined planes. *Eur. Phys. J.* B **15** (2), 357–369.

YIANTSIOS, S. G. & HIGGINS, B. G. 1989 Rayleigh–Taylor instability in thin viscous films. *Phys. Fluids* **1** (9), 1484–1501.